Shahrood University of Technology

Journal of Hydraulic and Water Engineering (JHWE)

Journal homepage: https://jhwe.shahroodut.ac.ir

Iranian Hydraulic Association (IHA)

Spatiotemporal Trend Analysis of Minimum, Mean, and Maximum Air Temperature in the Kashkan River Basin using Cloud Computing and Modified Mann–Kendall Tests

Hasan Torabi Poudeh[1,*]

[1] Department of Water Engineering, College of Agriculture, Lorestan University, Khorramabad, Iran

Article Info

Article history:

Received 2 June 2026
Received in revised form 20 June 2026
Accepted 28 June 2026
Published online 3 July 2026

DOI:
10.22044/jhwe.2026.17774.1090

Keywords
Kashkan River Basin
Spatiotemporal trend analysis
Air temperature
Tmin
Tmean
Tmax
Mann–Kendall test

Abstract

This study investigates the spatiotemporal trends of minimum, mean, and maximum temperature in the Kashkan Basin using nonparametric time-series tests, including the Mann–Kendall test modified by the PW_MK, VCA, and TFPW approaches, along with Sen's slope estimator. The results indicate that, at the annual scale, all three temperature variables exhibit statistically significant increasing trends. Specifically, mean temperature increased at a Sen's slope of 0.053 °C per year, minimum temperature at 0.051 °C per year, and maximum temperature at 0.056 °C per year. The Mann–Kendall test statistics for the annual data also confirm the high significance of these trends, indicating very high confidence levels for all variables. At the seasonal scale, increasing trends dominated most months and seasons, although their magnitude and statistical significance differed among variables. For mean temperature, the strongest increasing trends were observed in winter months and late spring, particularly in Esfand (March), Bahman (February), and Khordad (June), where high Z values and confidence levels confirmed warming. For minimum temperature, the greatest increases occurred during the warm months, particularly Tir (July), Mordad (August), Shahrivar (September), and the summer season. Maximum temperature also showed an upward trend in most months, with more pronounced increases in winter and early spring. Only in a few limited periods, such as Shahrivar (September) or Mordad (August) in some indices, decreasing or non-significant trends were observed. A comparison of the different trend-test methods shows that the overall pattern of temperature change in the Kashkan Basin is robust and consistently upward. The concurrent increases in minimum and maximum temperatures, in line with mean temperature, indicate an intensification of regional warming. Overall, the findings suggest that the Kashkan Basin has experienced a widespread and statistically significant warming trend in recent decades, with important implications for water resources, evapotranspiration, heat stress, and ecosystem stability in the region.

1. Introduction

Climate warming has increasingly manifested in altered thermal regimes, with consequences that extend beyond atmospheric conditions to affect hydrological processes, agricultural productivity, and ecosystem resilience. Minimum, mean, and maximum air

* *Corresponding author:* torabi.ha@lu.ac.irr, Fax: +98 6633235160, Tel:+989132205169

temperatures represent complementary indicators of this change; considered together, they provide a more complete diagnosis of whether changes in nocturnal cooling, daytime heating, or background thermal conditions drive warming. For this reason, their simultaneous analysis is essential for robust spatiotemporal climate assessment, particularly in semi-arid and topographically complex basins that are highly sensitive to climatic perturbations (Tabari et al., 2011). Recent advances in thermal remote sensing and reanalysis products have enabled long-term and spatially continuous monitoring of temperature dynamics. Among these, land surface temperature (LST) has become a key variable in climate–environment research. Studies have shown that LST products derived from MODIS and Landsat are particularly useful for characterizing thermal patterns, detecting temporal trends, and examining the relationships between temperature behavior and land-surface properties (Sobrino et al., 2004; Wan, 2008; Li et al., 2013). In addition, regional studies have demonstrated that LST can support near-surface air-temperature estimation, although its performance depends on environmental conditions, land-cover structure, and local ecological settings (Benali et al., 2012; Vancutsem et al., 2010). However, thermal behavior at the land–atmosphere interface is not controlled by climate alone. It is also shaped by land-use and land-cover change, vegetation dynamics, moisture availability, and topographic heterogeneity. Built-up expansion has been shown to increase LST and intensify urban heat island effects (Weng et al., 2004; Alshehri et al., 2023), while vegetation and precipitation exert strong moderating influences on surface thermal conditions (Nega et al., 2019; Meshesha et al., 2024). In semi-arid landscapes, thermal and vegetation indices are widely used to assess land degradation and desertification processes (Kumar et al., 2022). Likewise, elevation, slope, and aspect can substantially shape thermal variability in rugged terrain, making topography a critical determinant of spatial temperature patterns (Khandelwal et al., 2016; Ullah et al., 2023). In parallel with these data developments, cloud-based geospatial platforms—particularly Google Earth Engine—have transformed the analysis of large-scale climate and remote-sensing datasets by enabling scalable, reproducible processing of long time series and extensive spatial archives (Roy & Bari, 2022). In such contexts, nonparametric statistical methods are especially valuable because temperature records commonly exhibit non-normality, internal variability, and temporal non-stationarity. Accordingly, robust nonparametric trend tests provide a suitable methodological basis for identifying long-term temperature changes and assessing their significance in regional climate studies (Tabari et al., 2011). Despite these advances, three important gaps remain in the literature. First, most studies have been conducted at national or provincial scales, whereas river basins—as functional units of water and land management—have received comparatively less attention. Second, many investigations focus on a single thermal variable. However, integrated analysis of Tmin , Tmean , and Tmax is necessary for a fuller understanding of climate change. Third, basin-scale studies that explicitly combine cloud-computing infrastructure with statistical trend analysis remain limited (Li et al., 2013; Wan, 2008; Roy & Bari, 2022).

In line with the above discussion and with reference to the newly provided sources, the thermal trends in western Iranian basins such as Kashkan cannot be adequately analyzed without considering concurrent changes in streamflow, water quality, and land use; previous studies in the Karkheh, Dez, Karun, and Talar basins have demonstrated that temperature variations directly affect surface runoff, crop water demand, and pollutant concentrations (Torabi & Emamgholizadeh, 2015; Emamgholizadeh, 2015; Ruigar et al., 2024; Arabameri et al., 2025). Furthermore, forward-looking investigations using CMIP6 models and multi-criteria decision-making approaches emphasize that accurate temperature and precipitation forecasting is essential for simulating the combined effects of climate and land-use changes on basin water resources (Khoshnevisan et al., 2025; Ruigar et al., 2025). Hence, the integrated analysis of minimum, mean, and maximum temperatures alongside hydrological and water-quality variables can provide a more complete picture of the Kashkan Basin's vulnerability to climatic and anthropogenic stresses. Such an integrated framework would also offer a robust analytical basis for integrated water management and adaptation planning under future change scenarios.

Against this background, the Kashkan River Basin in western Iran provides an appropriate, management-relevant case for examining thermal change in response to climate variability and climate change. Owing to its elevation gradients, complex topography, heterogeneous land-surface properties, and strong dependence of water resources and agriculture on climatic conditions, the basin is likely highly sensitive to shifts in temperature regimes. Such shifts may influence evapotranspiration, crop water demand, snow persistence, runoff generation, and the timing of hydrological processes, with direct implications for water-resource management and agricultural planning. Given the established roles of topography, land use, and vegetation in shaping thermal behavior, notable spatial and temporal heterogeneity in temperature change is also expected within the basin (Khandelwal et al., 2016; Ullah et al., 2023; Roy & Bari, 2022). Accordingly, this study investigates the spatiotemporal dynamics of minimum, mean, and maximum temperatures in the Kashkan River Basin using long-term temperature data, cloud computing capabilities, and nonparametric trend tests. By integrating these approaches, the study aims to detect, quantify, and interpret thermal trends at the basin scale and to provide an analytical basis for water resource management, agricultural adaptation, and climate change planning in the Kashkan River Basin.

2. Material and Methods

2.1. Study area

The study was conducted in the Kashkan River Basin, one of the most significant sub-catchments of the Karkheh River, located in Lorestan Province, Western Iran (Fig. 1). The basin is geographically positioned within the UTM Zone 39N projection. Topographically, the area is characterized by the rugged terrain of the Zagros Mountains, with elevations ranging from a minimum of 529 m at the outlet to a peak of 3,605 m in the northern highlands. The drainage system follows a complex network, predominantly influenced by the regional tectonic structures and high-altitude precipitation patterns.

2.2. Google Earth Engine Cloud Computing Platform and Data Processing Workflow

Google Earth Engine (GEE) is an advanced web-based platform designed for processing geospatial data at the global scale. By leveraging Google’s massive computational infrastructure, it enables on-demand access and parallel processing of large volumes of satellite imagery and reanalysis products without the need to download or store massive datasets locally. In climate research, working with long-term time series (e.g., ERA5 reanalysis data) is often technically challenging due to the sheer volume of data (several terabytes) and the complexity of processing across multiple spatiotemporal scales, which can impose substantial hardware and computational constraints. By shifting computations to cloud servers, GEE eliminates storage-related limitations, improves the speed and efficiency of accessing climate variables, and provides a standardized framework for distributed, large-scale analyses.

2.3. Data Extraction and Processing Using Google Earth Engine and Python

In the first step, 2-m air temperature data were extracted from the ERA5-Land reanalysis dataset using Google Earth Engine (GEE). For this purpose, the boundary of the study area, corresponding to the downstream agricultural lands of the Koman Dam, was imported into the GEE environment as a vector layer. Spatial reducer functions were then applied to pixels within the study area to calculate weighted mean temperature values at daily, monthly, and annual time scales for the three variables: minimum temperature (Tmin), maximum temperature (Tmax), and mean temperature (Tmean). The resulting time series were subsequently extracted for further analysis. This approach, by overcoming the limitations associated with point-based observations and interpolation procedures commonly used in station-based methods, enabled the generation of consistent, continuous, and reliable climatic data for subsequent analyses.

To support detailed climatic analyses, a coherent, structured database comprising 8,766 daily records was developed for the three temperature variables—minimum, maximum, and mean—over the 26-year study period. The database was constructed in two main stages. In the first stage, two core columns, namely “Date” and “Temperature,” were directly extracted from the GEE environment, where dates were recorded in the Gregorian calendar and temperature values were stored as numerical observations. In the second stage, using Python and temporal and statistical processing procedures, seven additional columns were added to the dataset: Solar Year, Solar Month, Water Year, Season, Standard Score (Z-Score), Stress Index, and Group Code. As a result, the final database was organized as a 9-column table, the specifications of which are presented in Table 1. This database formed the primary basis for all subsequent analyses in the study. Following data completion and structuring, all additional processing and final analyses were conducted in the Python environment. At this stage, dedicated coding procedures were used to perform temperature trend analysis using nonparametric tests, estimate the rate of change, identify thermal anomalies, extract the frequency and persistence of stress periods, and generate the analytical indices, tables, and figures required for the study. Accordingly, Python in this research was used not only as a tool for database completion and organization, but also as the principal platform for statistical analyses, thermal stress assessment, and the production of the final research outputs. Overall, integrating Google Earth Engine as a platform for climatic data extraction and preprocessing, with Python as the environment for statistical analysis and modeling, provided an efficient, reproducible, and scalable framework for investigating the spatiotemporal variability of temperature within the study area. This framework can also be applied in similar climatological and hydrological studies.

Table 1. A sample of the data

Number	Time	Val	Year	Month	Season	Z	Is_stress	Group
1	2000-01-01 00:00:00	6.608	2000	1	Winter	-0.792	0	1
2	2000-01-02 00:00:00	6.512	2000	1	Winter	-0.802	0	1
3	2000-01-03 00:00:00	6.152	2000	1	Winter	-0.838	0	1
…….	…….	…….	…….	…….	…….	…….	…….	…….
…….	…….	…….	…….	…….	…….	…….	…….	…….
…….	…….	…….	…….	…….	…….	…….	…….	…….
9495	2025-12-30 00:00:00	-3.21	2025	12	Winter	-1.770	1	416
9496	2025-12-31 00:00:00	-1.87	2025	12	Winter	-1.637	1	416

2.4. Statistical Analysis using Python Programming

The data extracted in the previous stage were imported into the Python programming environment for advanced statistical analysis. Using specialized libraries such as Pandas and NumPy, data cleaning and restructuring were performed. Algorithms for the Mann-Kendall (MK) test and Sen's Slope estimator were coded to determine the direction and magnitude of trends. Furthermore, to mitigate statistical errors arising from serial autocorrelation, custom computational codes for Pre-Whitening (PW), Trend-Free Pre-Whitening (TFPW), and the Variance Correction Approach (VCA) were implemented. Finally, calculations for the Z-Score index were developed to monitor temperature anomalies.

2.5. Mann-Kendall (MK) Trend Test

In this study, the trends in monthly, seasonal, and annual streamflow time series for each station were analyzed using the non-parametric Mann-Kendall (MK) test. A fundamental prerequisite for the application of this test is the independence of data and the absence of significant serial autocorrelation

within the time series. Therefore, to ensure statistical validity, the effects of all significant autocorrelation coefficients were first removed using the Pre-Whitening (PW), Trend-Free Pre-Whitening (TFPW), and Variance Correction Approach (VCA) methods (detailed in the following sections). Subsequently, the MK test was applied to the modified, independent time series.

2.6. Mann-Kendall (MK) Test on Original Time Series (Non-Pre-Whitened)

The Mann-Kendall (MK) test is one of the most widely used non-parametric tests for trend analysis and is extensively applied to detect trends in hydrological time series. The null hypothesis (H0) assumes that the sample data. $\{X_i, i = ,2 \ldots, n\}$ are independent and identically distributed, while the alternative hypothesis (H1) indicates the presence of a monotonic trend in the data. To perform this test, the S statistic is first calculated using Equation (1), where x_j represents the jth data point, n is the total number of observations, and $\mathrm{sgn}(\theta)$ is the sign function, determined by Equation (2).

$$S = \sum_{i=1}^{n-1} \sum_{j=i+1}^{n} \mathrm{sgn}(x_j - x_i) \quad (1)$$

$$\mathrm{sgn}(\theta) = \begin{cases} 1 & \text{if } \theta > 0 \\ 0 & \text{if } \theta = 0 \\ -1 & \text{if } \theta < 0 \end{cases} \quad (2)$$

For $n \geq 8$, The S statistic follows an approximately normal distribution, where its mean and variance are calculated using Equation (3):

$$E(S) = 0 \quad \mathrm{Var}(S) = \frac{n(n-1)(2n+5) - \sum_{m=1}^{n} t_m(t_m - 1)(2t_m + 5)}{18} \quad (3)$$

where t_m denotes the number of equal (tied) observations in the ith group. The standardized Mann–Kendall test statistic, Z, is computed using Equation (4). The p-value (significance level) associated with the MK Z statistic can be obtained from the cumulative standard normal distribution.

$$Z = \begin{cases} \frac{S-1}{\sqrt{\mathrm{Var}(S)}} & S > 0 \\ 0 & S = 0 \\ \frac{S+1}{\sqrt{\mathrm{Var}(S)}} & S < 0 \end{cases} \quad (4)$$

2.7. MK Test on Pre-Whitened Time Series Using the von Storch Method (PW–MK)

Von Storch proposed this approach to remove serial autocorrelation, i.e., to *pre-whiten* the time series. In this method, the pre-whitened series is obtained using:

$$y_t = x_t - r_1 x_{t-1}$$

where r_1 is the lag-1 autocorrelation coefficient, x_t is the original time-series value at time t, and y_t is the pre-whitened series.

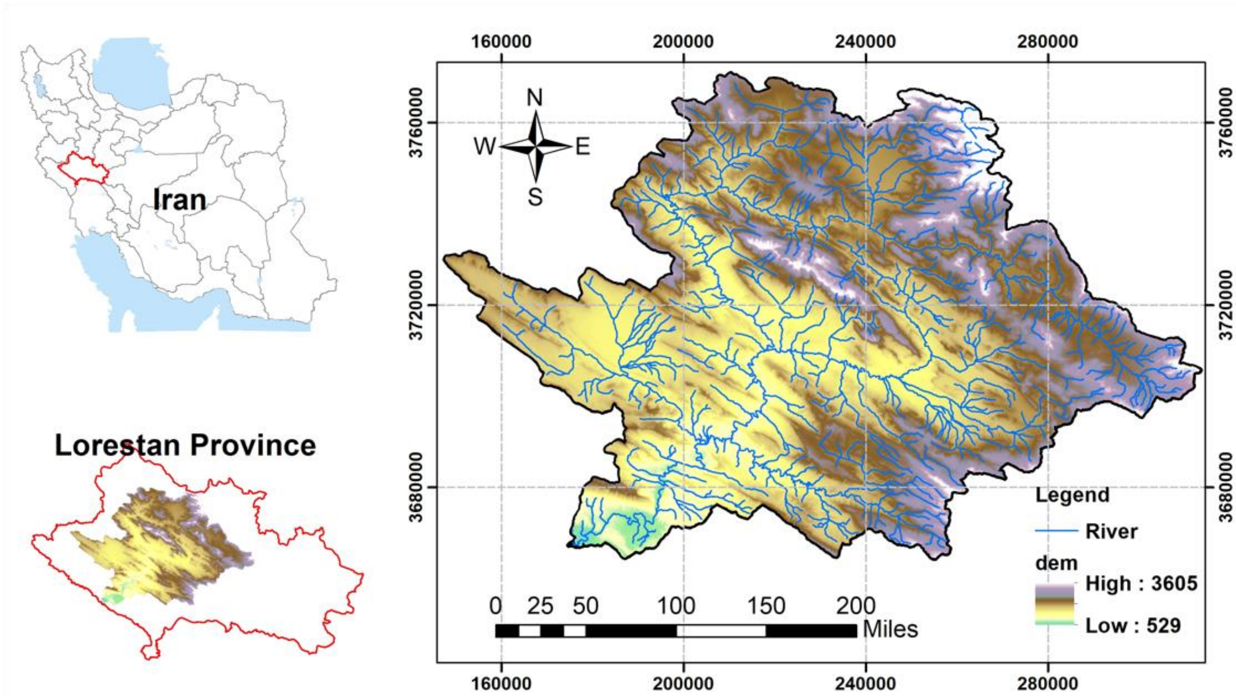

Figure 1. Study area

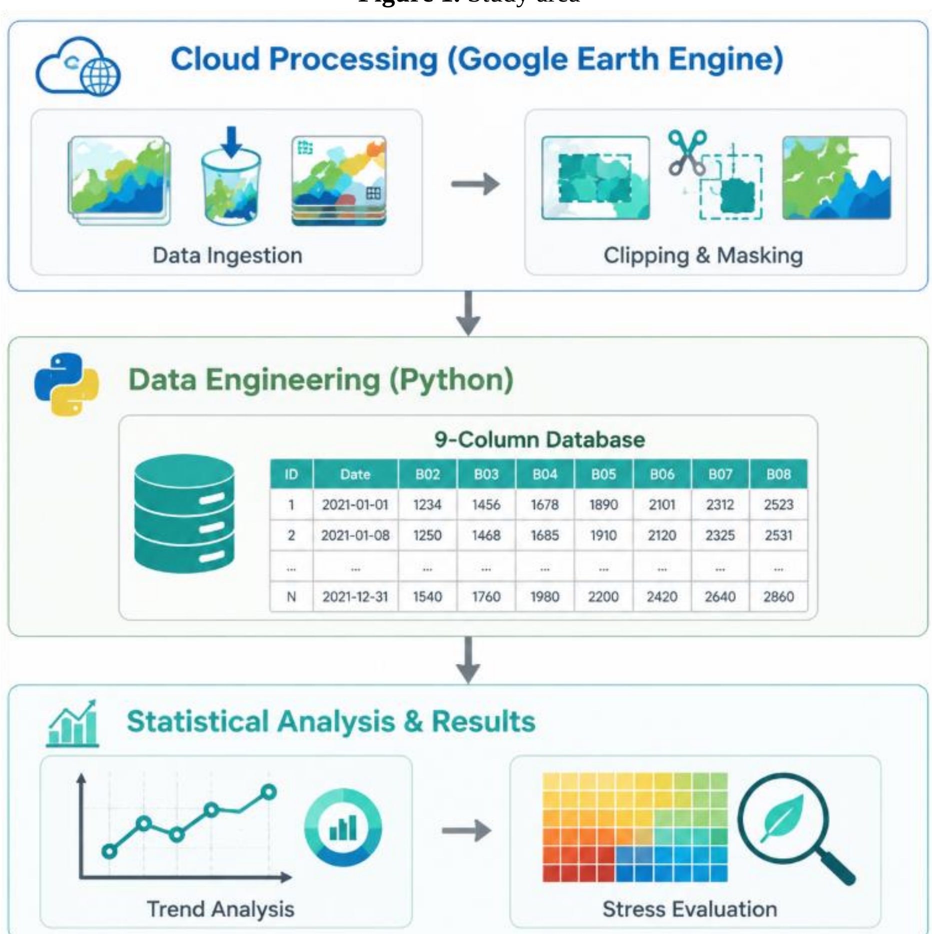

Figure 2. Methodological framework of the study

2.8. MK Test on Time Series with Variance Correction Approach (VCA)

This method was proposed by Hamed and Rao. In this approach, the effects of all significant autocorrelation coefficients at various lags are accounted for within the test. To achieve this, the modified variance is first calculated using Equation (5):

$$\mathrm{Var}^*(S) = \mathrm{Var}(S)\frac{n}{n^*}$$

$$Z^* = \begin{cases} \frac{S-1}{\sqrt{\mathrm{Var}^*(S)}} & S > 0 \\ 0 & S = 0 \\ \frac{S+1}{\sqrt{\mathrm{Var}^*(S)}} & S < 0 \end{cases} \qquad (5)$$

The correction factor is calculated according to Equation (6) :

$$\frac{n}{n^*} = 1 + \frac{2}{n(n-1)(n-2)}\sum_{k=1}^{n-1}(n-k)(n-k-1)(n-k-2)r_k^R \qquad (6)$$

r_k^R: the autocorrelation coefficient at lag k based on the ranked data. To compute r_k^R in Equation (7), the ranked data values, i.e. X_t, are substituted for RX_t.

$$r_k = \frac{\frac{1}{n-k}\sum_{t=1}^{n-k}[X_t - E(X_t)][X_{t+k} - E(X_t)]}{\frac{1}{n}\sum_{t=1}^{n}[X_t - E(X_t)]^2}$$

$$E(X_t) = \frac{1}{n}\sum_{t=1}^{n} X_t \qquad (7)$$

2.9. MK Test on Pre-Whitened Time Series using TFPW Method

The TFPW-MK method for detecting trends in autocorrelated time series was introduced by Yue et al. (2002) as follows:

1.The trend slope in the sample data is estimated using the Theil-Sen Approach (TSA) as follows:

$$b = \mathrm{Median}\left(\frac{X_j - X_l}{j-l}\right) \quad \forall l < j \qquad (8)$$

2. If the slope is approximately equal to zero, there is no need to continue the trend analysis. However, if its value is not equal to zero, the trend is assumed to be linear, and the sample data are detrended as follows:

$$X'_t = X_t - T_t = X_t - bt$$

3. The lag-1 autocorrelation coefficient of the detrended series X'_t is estimated using the following equations.

$$r_k = \frac{\frac{1}{n-k}\sum_{t=1}^{n-k}[X'_t - E(X'_t)][X_{t+k} - E(X'_t)]}{\frac{1}{n}\sum_{t=1}^{n}[X'_t - E(X'_t)]^2}$$

$$E(X'_t) = \frac{1}{n}\sum_{1}^{n} X'_t \qquad (9)$$

Where r_1 is the lag-1 autocorrelation coefficient of the detrended series X'_t, and $E(X'_t)$ represents the mean of the sample data.

4. After calculating the lag-1 autocorrelation coefficient, the first-order autoregressive process AR(1) is removed using the relationship $Y'_t = X'_t - r_1 X'_{t-1}$. This procedure is referred to as the Trend-Free Pre-Whitening (TFPW) method. The residual series obtained after applying TFPW is an independent series.

5. The identified trend T_t and the residual series Y'_t are recombined as $Y_t = Y'_t + T_t$. Consequently, the resulting series Y'_t preserves the original trend while eliminating the effect of autocorrelation.

6. The Mann-Kendall (MK) test is performed on the blended series Y_t to estimate the significance of the actual trend. The methodological framework of the study is shown in Figure 2.

Table 2. The summary statistics of the processed temperature data of Kashkan Basin.

Indicator	T_{min}	T_{max}	T_{mean}
Number of records	9,497	9,497	9,497
Number of columns	9	9	9
Time period	2000-01-01 to 2025-12-31	2000-01-01 to 2025-12-31	2000-01-01 to 2025-12-31
Missing values in time column	0	0	0
Total missing values in dataset	0	0	0
Mean temperature (val_mean)	7.524087	20.541391	14.562194
Temperature standard deviation (val_std)	8.556716	10.903012	10.039248
Minimum temperature (val_min)	-21.783	-7.781	-14.04
Maximum temperature (val_max)	24.048	39.331	31.378
Mean Z	approximately 0	approximately 0	approximately 0
Standard deviation of Z	1	1	1
Minimum Z	-3.425039	-2.597667	-2.849037
Maximum Z	1.931105	1.723341	1.675007
Number of days with Z≥1	2072	2262	2242
Number of days with Z≤−1	1867	2027	2005
Number of days with Z≥2	0	0	0
Number of days with Z≤−2	140	31	56
Number of stress days (is_stress=1)	1900	1900	1900
Number of stress days (is_stress=1)	1900	1900	1900
Number of non-stress days (is_stress=0)	7597	7597	7597
Stress rate	0.200063	0.200063	0.200063

3. Results and Discussion

3.1. Heat Stress Analysis Using the Z-Score Index in the Kashkan Basin

As presented in Table 2, the summary statistics of the processed temperature data provide the basis for evaluating thermal stress conditions in the Kashkan Basin. To complement the assessment of temperature variations, the Z-Score index was employed to identify thermal anomalies and the intensity of stress in the three time series of minimum temperature (Tmin), maximum temperature (Tmax), and mean temperature (Tmean). The results indicated that for all three variables, the data cover the period from 1 January 2000 to 31 December 2025, comprising 9,497 daily records, with no missing values in the time column or in the dataset as a whole.

- Number of records: Represents the total number of recorded data points (samples) in the database.
- Number of columns: Indicates the number of features or data columns available in the dataset for each variable.
- Time period: Specifies the exact start and end dates of the data collection period.
- Missing values in time column: Shows the number of missing or unrecorded entries in the time column (which is zero in this case).
- Total missing values in dataset: Quantifies the total number of empty or missing cells throughout the entire dataset.

- Mean temperature (val_mean): Represents the arithmetic mean of all temperature values recorded during the period.
- Temperature standard deviation (val_std): Describes the dispersion and fluctuations of temperature relative to the mean.
- Minimum temperature (val_min): The lowest temperature recorded (coldest point) in the entire time frame.
- Maximum temperature (val_max): The highest temperature recorded (hottest point) in the entire time frame.
- Mean Z: The average of the standardized scores (Z-scores), which is close to zero in normalized data.
- Standard deviation of Z: The standard deviation of the standardized scores, which is equal to 1 in the normalization process.
- Minimum Z: Indicates the distance of the minimum temperature from the mean, expressed in units of standard deviation.
- Maximum Z: Indicates the distance of the maximum temperature from the mean, expressed in units of standard deviation.
- Number of days with $Z \geq 1$: The number of days where the temperature was more than one standard deviation above the mean.
- Number of days with $Z \leq -1$: The number of days where the temperature was more than one standard deviation below the mean.
- Number of days with $Z \geq 2$: The number of days with extreme heat (more than two standard deviations above the mean).
- Number of days with $Z \leq -2$: The number of days with extreme cold (more than two standard deviations below the mean).
- Number of stress days (is_stress=1): The total number of days classified as being in a “stress” condition based on defined criteria.
- Number of non-stress days (is_stress=0): The number of days classified as having normal temperature conditions (no stress).

Stress rate: The ratio of stress days to the total number of days in the period, expressed as a decimal. Examination of the descriptive statistics showed that the mean minimum, maximum, and mean temperatures were 7.524°C, 20.541°C, and 14.562°C, respectively. The range of variation in these three variables was also considerable. The recorded minimum and maximum values were -21.783°C to 24.048°C for Tmin, -7.781°C to 39.331°C for Tmax, and -14.040°C to 31.378°C for Tmean. This range indicates that the Kashkan Basin experienced
substantial thermal fluctuations during the study period. The analysis of the standardized Z index further showed that the mean Z value across all three series was approximately zero, with a standard deviation of 1, indicating that the data were properly standardized. Nevertheless, the extreme Z values indicated that the intensity of negative anomalies was greater in the minimum-temperature series than in the other two. Specifically, the minimum Z value in Tmin reached -3.425, whereas the corresponding values for Tmax and Tmean were -2.598 and -2.849, respectively. In addition, the number of severe cold events with the threshold $Z \leq -2$ was 140 days for Tmin, 56 days for Tmean, and 31 days for Tmax. These findings indicate that severe thermal stress events in the Kashkan Basin were more pronounced in the minimum-temperature series, suggesting that extremely cold nights or sharp nocturnal temperature drops played a more important role in shaping thermal anomalies.
In terms of stress-event frequency, the is_stress index showed that in each of the three time series, 1,900 days were classified as stress days, equivalent to 20.0063% of the entire study period. This indicates that nearly one-fifth of all days in the Kashkan Basin experienced thermal

stress. The identical stress rate across all three series further suggests that the stress classification was applied consistently to Tmin, Tmax, and Tmean.

Overall, the findings from the Z-Score index indicate that, in addition to pronounced temperature variability, the Kashkan Basin has experienced a high frequency of thermal stress events. The severity of these anomalies was greater in the minimum temperature series than in the other variables, which may reflect the basin's higher vulnerability to nocturnal cooling and extreme cold events. From this perspective, the obtained results can be used to assess the climatic impacts on water resources, evapotranspiration, and agricultural productivity in the Kashkan Basin.

3.2.Trend analysis of air temperature changes in the Kashkan Basin

The multi-scale thermal assessment of the Kashkan Basin over 2000–2025 reveals a clear shift toward warmer temperature regimes across annual, seasonal, and monthly scales. The analysis of maximum temperature (Fig. 3, Table 3) indicates an intensification of daytime heat during mid-summer (especially July–August), together with a higher recurrence of warm extremes in recent years; the temporal heat patterns also suggest that elevated temperatures increasingly extend into the transitional months (May and September), implying a lengthening of the warm season and prolonged daytime thermal stress. Consistently, the mean temperature results (Fig. 4, Table 4) confirm an overall upward displacement of the basin's thermal baseline at the annual scale, reflected in higher seasonal averages and a systematic warming of the central tendency across months. The most pronounced and critical signal, however, emerges from minimum-temperature behavior (Fig. 5, Table 5), where the stronger upward trend in nighttime temperatures points to enhanced nocturnal warming and a weakening contraction of the cold season. From an impacts perspective, these combined signals—especially accelerated Tmin warming—are expected to increase evaporative demand, alter hydrological balance, and exacerbate risks to water resources and agriculture by extending and intensifying thermal stress in the Kashkan Basin.

One of the main challenges in detecting temperature trends in climatic time series is the presence of short-term persistence and serial correlation, which can inflate the apparent significance of the Mann–Kendall test and lead to spurious inferences. Accordingly, in this study, trend results were evaluated not only in the original form (Origin) but also under corrective approaches including pre-whitening (PW), trend-free pre-whitening (TFPW), and variance correction (VCA) to assess the robustness of detected trends against autocorrelation effects. The comparison indicates that although PW reduces the magnitude of the Z statistic relative to the Origin case in some months and seasons, the convergence of results between TFPW and VCA and the persistence of statistically significant Z values at high confidence levels demonstrate that the warming signal is physically real rather than a statistical artifact. Specifically, at the annual scale for maximum temperature (Tmax), an

increasing trend with a slope of about 0.06 ∘C/yr is reported, and its significance remains stable after corrections (Origin: Z=3.26, P=99.9; PW: Z=2.97, P=99.7%; VCA: Z=2.54, P=98.9%; TFPW: Z=3.25,

of cold-season conditions. The corresponding distributional plots show an upward shift in winter and autumn temperature quartiles and a reduction in the occurrence/intensity of very cold values, collectively indicating a P=99.9%). This statistical stability, together with the concentration of strong signals in the warm season, indicates that Tmax warming is particularly pronounced in summer; for instance, the summer Z equals 4.10 in Origin and 4.41 in TFPW (both at P=99.9%), implying intensified heat stress during the period of peak water demand and the most temperature-sensitive phenological stages of crops. At the monthly scale, July through September show the strongest and most persistent trends; for example, July remains highly significant (Origin: Z=3.31; TFPW: Z=3.76), August also exhibits robust significance (Origin: Z=3.00; TFPW: Z=3.06), and September is similarly strong (Origin: Z=3.44; TFPW: Z=3.29), consistently at very high confidence levels.

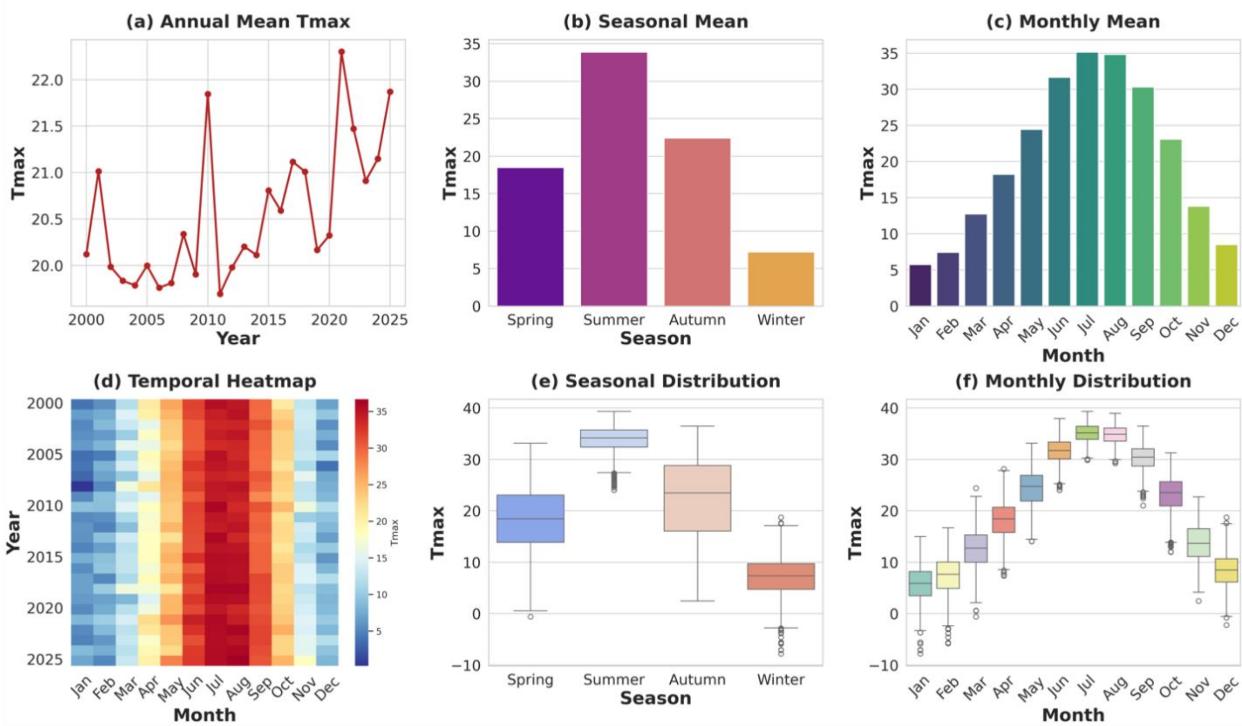

Figure 3. Multi-scale Thermal Analysis Summary (Tmax)

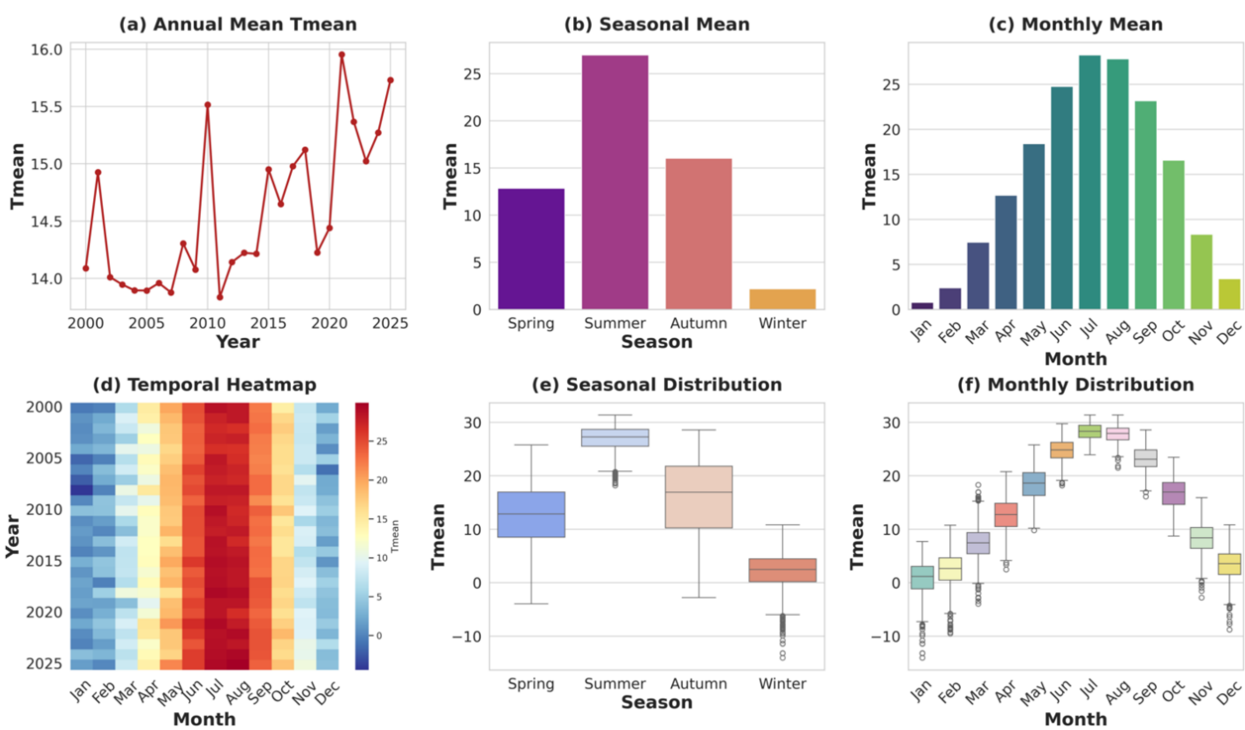

Figure 4. Multi-scale Thermal Analysis Summary (Tmean)

For mean temperature (Tmean), the overall warming pattern is likewise confirmed, with an annual slope of approximately 0.057 ∘C/yr. The annual Z equals 3.6589 in Origin with P=99.9%, and the trend remains significant after corrections (PW: Z=2.919, P=99.64%; VCA: Z=2.7568, P=99.41%; TFPW: Z=3.7601, P=99.9%). Seasonally, summer emerges as the primary hotspot of Tmean

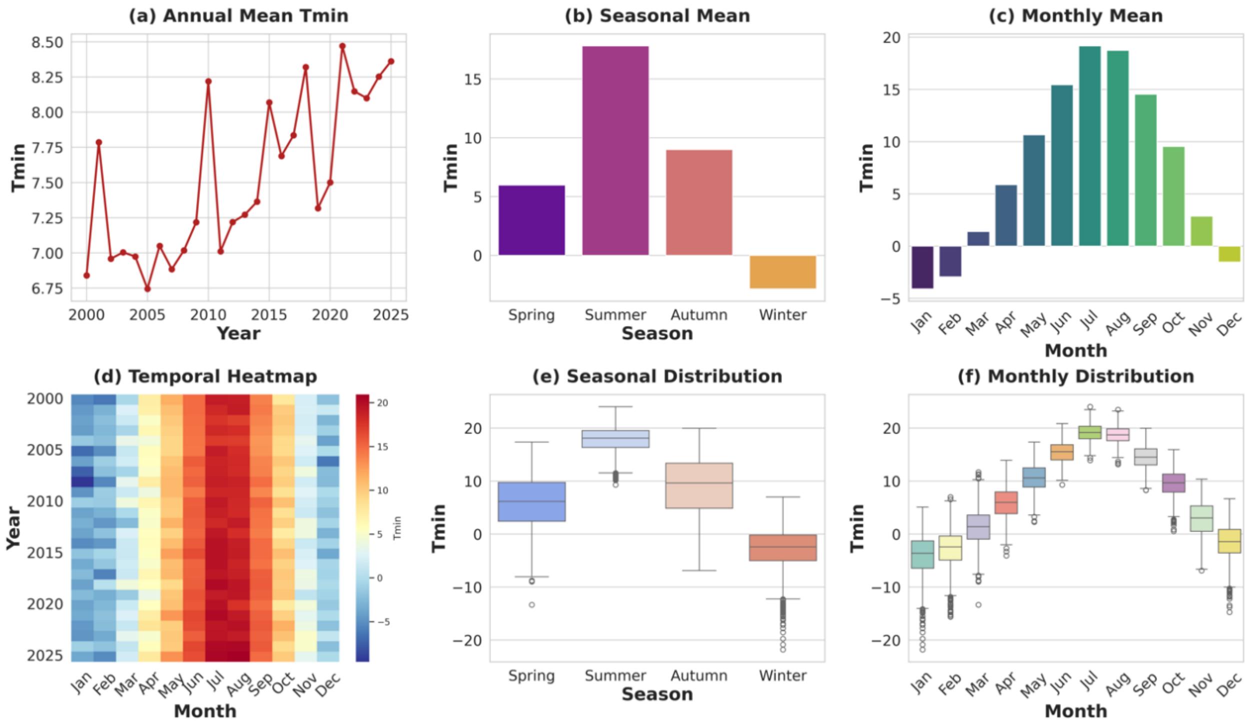

Figure 5. Multi-scale Thermal Analysis Summary (Tmin)

warming, with Z=4.72 in Origin and Z=5.02 in TFPW (both at P=99.9%), indicating intensified warming during the warmest part of the year. At the monthly scale, late spring and summer exhibit strong signals as well; however, May is weak and not statistically robust, whereas June through September show the clearest warming signals, with July, August, and September standing out as the most persistent warm-season months. The minimum temperature behavior (Tmin) indicates that nighttime warming is particularly strong and ecophysiologically important. At the annual scale, Tmin increases with a slope of about 0.06 ∘C/yr and exhibits very high significance (Origin: Z=4.58, P=99.9%; PW: Z=2.83, P=99.5%; VCA: Z=3.36, P=99.9%; TFPW: Z=4.32, P=99.9). Seasonally, summer records the strongest Tmin trend (Origin: Z=5.03, P=99.9%; TFPW: Z=5.02, P=99.9%), while autumn also remains significant (Origin: Z=2.69, P=99.3%; TFPW: Z=2.22, P=97.3%). In the combined interpretation of the three variables, the substantial warming in Tmin across multiple time scales suggests a tendency toward reduced diurnal temperature range (DTR). However, this inference would be stronger if directly confirmed by DTR analysis. Overall, the persistence of significant Z statistics after applying TFPW and VCA across monthly, seasonal, and annual scales in all three tables confirms the robustness of the findings and supports interpreting the observed warming as a systematic climatic shift rather than short-term variability, thereby reinforcing the need to revise cropping calendars, adopt heat-tolerant cultivars, and implement adaptive water-resource management.

4. Conclusion

A comprehensive analysis of mean temperature trends indicates that warming in the study area is a dominant and systematic phenomenon, with an upward trend confirmed with high confidence across all test methods (Original, VCA, and TFPW) at the annual scale. Among the time intervals, summer , with the highest statistical significance, is considered the primary driver of this climate change. The stability of the test statistics after applying correction methods to remove the effects of autocorrelation—particularly TFPW and VCA—demonstrates that the observed warming is not a random fluctuation but a structural, real climatic shift that requires special attention in water resource management planning and agricultural adaptation

Table 3. Statistical analysis of max temperature (Tmax) trends using original and autocorrelation-corrected (PW, VCA, TFPW) Mann-Kendall tests at monthly, seasonal, and annual scales.

		R				Origin		PW MK						VCA		FTPW	
Seri Name	AR	Upper	Lower	Slope	Pc	Z	P	R	Slope	PC	Z	P	n/n	Z	P	Z	P
Jan	0.19	-0.36	0.28	0.10	955	1.90	94.2	0.04	0.07	655	1.19	76.8	1.16	1.76	92.2	1.52	87.0
Feb	-0.28	-0.36	0.28	0.05	456	0.75	54.4	-0.08	0.03	348	0.72	53.2	0.51	1.05	70.4	0.49	37.9
Mar	-0.48	-0.36	0.28	-0.02	-227	-0.31	24.0	-0.04	-0.05	-492	-1.00	68.5	0.10	-0.97	67.1	-0.91	64.0
Apr	-0.04	-0.36	0.28	0.06	555	0.62	46.2	-0.08	0.07	738	1.33	81.8	0.81	0.69	50.7	1.33	81.8
May	-0.13	-0.36	0.28	0.01	135	0.22	17.8	-0.09	0.03	344	0.82	58.5	0.90	0.23	18.6	0.77	56.2
Jun	0.06	-0.36	0.28	0.05	508	1.72	91.4	-0.01	0.05	545	1.85	93.5	0.83	1.89	94.1	2.03	95.8
Jul	0.37	-0.36	0.28	0.06	645	3.31	99.9	-0.05	0.06	593	2.31	97.9	1.58	2.63	99.2	3.76	99.9
Aug	0.36	-0.36	0.28	0.07	723	3.00	99.7	0.04	0.06	571	1.99	95.3	1.72	2.29	97.8	3.06	99.8
Sep	0.42	-0.36	0.28	0.07	726	3.44	99.9	-0.14	0.05	524	1.99	95.3	1.85	2.53	98.9	3.29	99.9
Oct	0.06	-0.36	0.28	0.04	423	1.32	81.5	0.03	0.02	243	0.77	56.2	1.12	1.25	78.7	0.82	58.5
Nov	-0.03	-0.36	0.28	0.10	960	2.29	97.8	0.00	0.10	1027	2.08	96.2	1.01	2.29	97.8	1.99	95.3
Dec	-0.13	-0.36	0.28	0.09	935	2.03	95.7	0.05	0.12	1190	1.99	95.3	0.86	2.18	97.1	1.85	93.5
Winter	-0.30	-0.36	0.28	0.04	434	1.01	69.0	-0.05	0.03	283	0.68	50.0	0.45	1.51	86.8	0.35	27.7
Spring	0.04	-0.36	0.28	0.04	364	1.10	73.1	-0.04	0.06	571	1.61	89.4	0.92	1.15	74.8	1.80	92.7
Summer	0.66	-0.36	0.28	0.07	719	4.10	99.9	-0.16	0.04	353	2.50	98.7	2.15	2.79	99.5	4.41	99.9
Autumn	0.00	-0.36	0.28	0.10	968	2.69	99.3	0.02	0.09	858	2.31	97.9	1.07	2.60	99.1	2.03	95.8
year	0.29	-0.36	0.28	0.06	590	3.26	99.9	0.00	0.05	485	2.97	99.7	1.66	2.54	98.9	3.25	99.9

Table 4. Statistical analysis of mean temperature (Tmean) trends using original and autocorrelation-corrected (PW, VCA, TFPW) Mann-Kendall tests at monthly, seasonal, and annual scales.

		R				Origin		PW MK						VCA		FTPW	
Seri Name	AR	Upper	Lower	Slope	Pc	Z	P	R	Slope	PC	Z	P	n/n	Z	P	Z	P
Jan	0.21	-0.36	0.28	0.08	776	1.81	92.9	0.01	0.04	393	0.82	58.5	1.12	1.71	91.18	1.33	81.81
Feb	-0.37	-0.36	0.28	0.04	372	0.97	66.6	-0.20	0.03	286	0.49	37.9	0.45	1.44	84.87	0.26	20.13
Mar	-0.47	-0.36	0.28	-0.01	-62	-0.04	3.6	-0.07	-0.03	-300	-0.58	44.1	0.08	-0.16	12.32	-0.54	40.73
Apr	-0.04	-0.36	0.28	0.03	327	0.53	40.0	-0.09	0.05	464	1.10	72.6	0.79	0.60	44.81	1.05	70.85
May	-0.09	-0.36	0.28	0.00	44	0.26	20.9	-0.07	0.02	220	0.58	44.1	0.96	0.27	21.67	0.58	44.14
Jun	0.19	-0.36	0.28	0.06	584	2.38	98.3	-0.04	0.06	581	2.36	98.2	1.10	2.27	97.65	2.69	99.27
Jul	0.52	-0.36	0.28	0.08	762	4.06	99.9	-0.12	0.05	547	2.73	99.4	1.98	2.89	99.61	4.51	99.90
Aug	0.42	-0.36	0.28	0.08	847	3.26	99.9	0.04	0.07	689	2.50	98.7	1.82	2.42	98.42	3.53	99.90
Sep	0.58	-0.36	0.28	0.09	869	3.61	99.9	-0.19	0.04	366	1.99	95.3	1.99	2.57	98.97	3.57	99.90
Oct	0.04	-0.36	0.28	0.03	316	1.68	90.6	0.02	0.02	211	1.19	76.8	1.06	1.62	89.58	1.28	80.12
Nov	0.16	-0.36	0.28	0.09	866	2.56	98.9	-0.01	0.08	843	2.27	97.7	1.18	2.35	98.10	2.64	99.16
Dec	-0.24	-0.36	0.28	0.07	740	1.50	86.5	0.13	0.09	916	1.85	93.49	0.51	2.10	96.47	1.33	81.81
Winter	-0.32	-0.36	0.28	0.05	465	1.19	76.8	-0.07	0.04	406	1.14	74.8	0.37	1.95	94.82	0.82	58.49
Spring	0.07	-0.36	0.28	0.03	299	0.93	64.5	-0.02	0.05	497	1.38	83.1	0.92	0.97	66.55	1.52	87.02
Summer	0.70	-0.36	0.28	0.08	828	4.72	99.9	-0.16	0.04	363	2.27	97.7	2.24	3.15	99.90	5.02	99.90
Autumn	0.07	-0.36	0.28	0.08	759	2.78	99.5	0.02	0.07	696	2.27	97.7	1.15	2.59	99.05	2.31	97.94
year	0.39	-0.36	0.28	0.06	565	3.66	99.9	-0.03	0.04	386	2.92	99.64	1.76	2.76	99.41	3.76	99.90

Table 5. Statistical analysis of min temperature (Tmin) trends using original and autocorrelation-corrected (PW, VCA, TFPW) Mann-Kendall tests at monthly, seasonal, and annual scales.

		R				Origin		PW MK						VCA		FTPW	
Seri Name	AR	Upper	Lower	Slope	Pc	Z	P	R	Slope	PC	Z	P	n/n	Z	P	Z	P
Jan	0.16	-0.36	0.28	0.05	501	1.72	91.4	-0.01	0.02	179	0.63	47.5	1.15	1.60	89.2	1.19	76.8
Feb	-0.40	-0.36	0.28	0.01	144	0.44	34.4	-0.32	0.01	57	0.26	20.1	0.29	0.82	58.5	0.12	9.2
Mar	-0.34	-0.36	0.28	0.01	136	0.35	27.7	-0.06	0.00	-24	-0.07	6.0	0.00	5.25	99.9	-0.07	6.0
Apr	-0.08	-0.36	0.28	0.00	23	0.09	6.8	-0.10	0.01	139	0.82	58.5	0.67	0.11	8.4	0.82	58.5
May	0.03	-0.36	0.28	0.02	216	0.71	51.9	0.00	0.03	309	1.14	74.8	1.17	0.65	48.8	1.14	74.8
Jun	0.54	-0.36	0.28	0.07	710	4.14	99.9	-0.16	0.04	386	2.22	97.3	1.97	2.95	99.7	4.04	99.9
Jul	0.58	-0.36	0.28	0.09	870	4.32	99.9	-0.16	0.05	475	2.55	98.9	2.18	2.93	99.7	4.51	99.9
Aug	0.43	-0.36	0.28	0.08	808	3.66	99.9	0.02	0.06	558	2.78	99.5	1.74	2.77	99.5	4.04	99.9
Sep	0.71	-0.36	0.28	0.09	923	4.36	99.9	-0.31	0.03	272	1.38	83.1	2.23	2.92	99.7	4.32	99.9
Oct	-0.12	-0.36	0.28	0.03	301	1.01	69.0	-0.02	0.02	213	0.72	53.2	0.67	1.24	78.7	0.58	44.1
Nov	0.14	-0.36	0.28	0.08	817	2.20	97.3	-0.02	0.07	735	1.85	93.5	0.99	2.21	97.3	2.03	95.8
Dec	-0.34	-0.36	0.28	0.05	464	1.10	73.1	0.17	0.07	674	1.89	94.2	0.16	2.79	99.5	1.61	89.4
Winter	-0.23	-0.36	0.28	0.04	448	1.41	84.3	-0.07	0.04	373	1.14	74.8	0.43	2.15	96.8	0.86	61.3
Spring	0.20	-0.36	0.28	0.04	363	1.76	92.2	0.05	0.04	387	1.94	94.7	1.32	1.53	87.5	2.27	97.7
Summer	0.71	-0.36	0.28	0.09	885	5.03	99.9	-0.18	0.03	288	2.08	96.2	2.36	3.27	99.9	5.02	99.9
Autumn	0.05	-0.36	0.28	0.05	509	2.69	99.3	0.04	0.05	457	2.08	96.2	1.02	2.66	99.2	2.22	97.3
year	0.48	-0.36	0.28	0.06	577	4.58	99.9	-0.06	0.03	340	2.83	99.5	1.86	3.36	99.9	4.32	99.9

Reservoir sedimentation is the main issue for most of the reservoirs around the world. Dez Reservoir is one of the largest reservoirs in Iran, which suffers from sedimentation problems. The main reasons of sedimentation in this reservoir (and also similar reservoirs, which are located in arid and semi-arid areas) are scarce vegetation cover, steep topography, and intense rainfall. In Dez Reservoir, the sedimentation issue could be controlled by applying different strategies, including watershed management, sluicing, releasing density currents, free and pressure flushing, and sediment bypass. Sedimentation could be reduced by 11-15% with density current venting, and by 2% with pressure flushing. Free flushing and sluicing are not recommended due to 1) their negative effects on the downstream ecosystem, and 2) lack of low-level outlets in Dez Dam. The pressure flushing method for removing sediments can be localized, and thus it is the recommended method when there is a need for localized removal of deposited sediments such as sediments around a water intake inlet. To use the hydraulic flushing, sluicing and density current venting methods efficiently, the bottom outlets should be designed with sufficient capacity.

Data Availability

The data used to support the findings of this study are available from the corresponding author upon request.

Conflicts of Interest

The authors declare that they have no conflicts of interest regarding the publication of this paper.

References

Adam, N., Erpicum, S., Archambeau, P., Pirotton, M., & Dewals, B. (2015). Stochastic modelling of reservoir sedimentation in a semi-arid watershed. *Water Resources Management*, 29, 785–800.

Aksoy, H., & Kavvas, M. L. (2005). A review of hillslope and watershed scale erosion and sediment transport models. *Catena*, 64, 247–271.

Alatorre, L., Beguería, S., & García-Ruiz, J. M. (2010). Regional scale modeling of hillslope sediment delivery: A case study in the Barasona Reservoir watershed, Spain, using WATEM/SEDEM. *Journal of Hydrology*, 391, 109–123.

Alighalehbabakhani, F., Miller, C. J., Selegean, J. P., Barkach, J., Sadrian, S., & Darian, M.

(2017). Forecasting the remaining reservoir capacity in the Laurentian Great Lakes watershed. *Journal of Hydrology*, 555, 926–937.

Arabameri, A., Emamgholizadeh, S., Chaplot, B., & Zallaghi, E. (2025). Long-term spatiotemporal assessment of water quality in the Karun River, Southern Iran: A novel Python-based approach for rapid processing. *Water Quality Research Journal*, 60(1), 196–213.

De Roo, A., Offermans, R., & Cremers, N. L. (1996). A single-event physically-based hydrological and soil erosion model for drainage basins. II: Sensitivity analysis, validation and application. *Hydrological Processes*, 10, 1119–1126.

Dezab Acres. (2005). *Dez Dam rehabilitation project, task 1: Reservoir operation review & sediment study* (Report to Khuzestan Water and Power Authority, Ahwaz, Iran).

Emamgholizadeh, S. (2015). Trend analysis of stream flow changing of North watershed of Dez River with MK test with the TFPW-MK procedure. *Journal of Water and Soil Conservation*, 22(3), 39–55.

Emamgholizadeh, S., & Samadi, H. (2008). Desilting of deposited sediment at the upstream of the Dez Reservoir in Iran. *Journal of Applied Sciences in Environmental Sanitation*, 3, 25–35.

Jones, K., Berney, O., Carr, D., & Barrett, E. (1981). *Arid zone hydrology for agricultural development*. FAO Irrigation and Drainage.

Khoshnevisan, S., Emamgholizadeh, S., & Ashouri, R. (2025). Predicting temperature and precipitation changes in the Shahrood Region using CMIP6 climate models with a novel multi-criteria decision-making approach: OPLO-POCOD. *Advanced Technologies in Water Efficiency*.

Kondolf, G. M., Gao, Y., Annandale, G. W., Morris, G. L., Jiang, E., Zhang, J., ... & Yang, C. T. (2014). Sustainable sediment management in reservoirs and regulated rivers: Experiences from five continents. *Earth's Future*, 2, 256–280.

Lehner, B., Liermann, C. R., Revenga, C., Vörösmarty, C., Fekete, B., Crouzet, P., ... & Wisser, D. (2011). *Global reservoir and dam database: Technical documentation, version 1*.

Molina-Navarro, E., Martínez-Pérez, S., Sastre-Merlín, A., & Bienes-Allas, R. (2014). Catchment erosion and sediment delivery in a limno-reservoir basin using a simple methodology. *Water Resources Management*, 28, 2129–2143.

Morris, G. L., & Fan, J. (1998). *Reservoir sedimentation handbook: Design and management of dams, reservoirs, and watersheds for sustainable use*. McGraw-Hill Professional.

Rashid, M. U., Shakir, A. S., Khan, N. M., Latif, A., & Qureshi, M. M. (2015). Optimization of multiple reservoirs operation with consideration to sediment evacuation. *Water Resources Management*, 29, 2429–2450.

Ruigar, H., Emamgholizadeh, S., Gharechelou, S., & Golian, S. (2024). Evaluating the impacts of anthropogenic, climate, and land use changes on streamflow. *Journal of Water and Climate Change*, 15(4), 1885–1905.

Ruigar, H., Gharechelou, S., Emamgholizadeh, S., & Golian, S. (2025). Impact assessment of future land use and climate change on Talar River streamflow—Mazandaran, Iran: Ruigar et al. *Theoretical and Applied Climatology*, 156(4), 202.

Shuguang, L., Yonglai, Z., Zhengji, Z., & Congxian, L. (2002). Sediment load of Asian rivers flowing into the oceans and their regional variation.

Shukla, S., Jain, S. K., Kansal, M., & Chandniha, S. K. (2017). Assessment of sedimentation in Pong and Bhakra reservoirs in Himachal Pradesh, India, using geospatial technique. *Remote Sensing Applications: Society and Environment*, 8, 148–156.

Sumi, T., & Kantoush, S. A. (2010). Integrated management of reservoir sediment routing by flushing, replenishing, and bypassing sediments in Japanese river basins. In *Proceedings of the 8th International Symposium on Ecohydraulics* (pp. 831–838). Seoul, Korea.

Torabi, H., & Emamgholizadeh, D. S. (2015). Analysis of stream flow trend across Karkheh watershed and effect of autocorrelation coefficient on the trend of flow. *Iranian Water Research Journal*, 9(1), 143–151.

Yoon, Y. (1992). The state and the perspective of the direct sediment removal methods from reservoirs. *International Journal of Sediment Research*, 7, 99–115.